J Solid State Electrochem (2011) 15:917–929
DOI 10.1007/s10008-010-1086-9

REVIEW

Towards a unified description of the host–guest coupling in the course of insertion processes

Eduard V. Vakarin · Jean Pierre Badiali

Received: 18 February 2010 / Revised: 22 April 2010 / Accepted: 23 April 2010 / Published online: 8 May 2010

Abstract We present an integrated analysis concerning common aspects of various type insertion processes (cation intercalation in a host material, hydrogen sorption by metals), supplemented by the host volume expansion, staging, or restructuring. A description of such processes requires investigation of the coupling between the insertion statistics and the elastic properties of the host matrix. Various models for the coupling are reviewed. We show that the standard Frumkin isotherm has to be modified to take into account the stress and strain fields appearing upon the guest insertion, as well as the host-mediated interaction between them. Recent applications of such an approach to various systems are discussed. The equilibrium as well as transport properties are considered. For the collective diffusion, the driving force is not only the concentration gradient, but also the stress and strain gradients. The latter may have a local or a non-local character, which results in a non-Fickian diffusion detected experimentally. The thermodynamics of intercalation into disordered matrices is analyzed in terms of the maximum entropy principle combined with the distortive lattice gas model. Recent experimental results on the ionic insertion into disordered matrices are analyzed in this light.

Introduction

Intercalation of guest particles into host matrices is a basic problem, related to a design of rechargeable high-energy batteries, electrochromic devices (see [1] for a review), hydrogen-storage systems [2], and superconductors [3]. The insertion process can be viewed as adsorption of guest particles on the host lattice. In case of charged particles, the ionic charge inside the matrix is compensated by the electrons. For that reason, the electrochemical intercalation is also similar (at least, in some aspects) to a three-dimensional adsorption of neutral species. Based on this analogy the intercalation is traditionally described within the lattice gas (LG) model. In this approach, all the properties (intercalation isotherm or capacity–concentration--dependence) are connected by ordering the guest on different adsorption sites of a rigid host lattice—the *configurational* transitions. The LG-type models [4] work satisfactory if an effective interaction W between the intercalants does not depend on their concentration. For attractive interactions ($W<0$), the theory predicts sharp peaks [5] (capacity vs concentration). For repulsive interactions ($W>0$), the LG model predicts an order–disorder transition with a very broad peak. In situations when both peaks appear at different ionic concentrations x_0 and x_1, a piece-wise description [6] ($W<0$ around x_0 and $W>0$ around x_1) is used for fitting. But, in that case, one cannot answer why the interaction parameter changes sign with the concentration. Moreover, the LG description becomes inadequate [4] when the characteristic peaks are superimposed [7], like in layered Li_xTiS_2.

Host matrices can be filled by the guest particles in the course of different processes [1], such as exposing the host to the intercalant vapor (or liquid solution) or passing current through an electrochemical cell, with the host being one of the electrodes. In the course of the electrochemical intercalation, the guest ion insertion results from electronic and ionic exchange at the electrode/solution boundary. The solution usually contains a metal-ion bearing salt (e.g., $LiClO_4$) which dissociates into cations and anions. The cationic species is then inserted into the matrix (e.g., TiS_2),

E. V. Vakarin (✉) · J. P. Badiali
LECIME (UMR 7575), CNRS-ENSCP,
11 rue P. et M. Curie,
75231 Cedex 05 Paris, France
e-mail: eduard.vakarin@upmc.fr

where the ions are screened by the electronic species of the inorganic matrix. The matrix remains impenetrable for the other ionic component. Namely, positive ions (Li^+, for instance) are present in the solid matrix while a strong exclusion of the negative ions occurs. For this reason, one has to take into account the overall electroneutrality, thermodynamic equilibrium, and the *permselectivity* (or exclusion) effect. The latter implies a stepwise change of the ionic concentrations at the electrode/electrolyte interface. The exclusion is commonly discussed in application to ion-selective membranes [8] or electroactive polymer films [9] where the ionic transport is quite similar to that of the intercalation compounds. Therefore, the permselectivity [9] should be considered as an essential part of the intercalation which is different from an unconstrained deposition process. Nevertheless, the exclusion effect is beyond the scope of the LG model.

On the other hand, the insertion of the guest species induces the stress into the host matrix. This may lead to segregation effects [10] or even to instabilities [11] of the host–guest system. Also, a loading path is shown [12] to influence the guest uptake efficiency. Due to this, the host may undergo an expansion or local distortion. Typical examples are the hydrogen sorption by metals [12–15] or the intercalation of Li ions into layered materials [4, 7]. Quite often, the host undergoes structural transformations [6, 16–18] in the course of the intercalation. These are the *structural* transitions. In this case, the LG model implies several sublattices [4, 18] corresponding to each configuration of the host. However, such a restructuring suggests that elastic effects are never negligible. Indeed, in graphite compounds, these effects result in the staging phenomenon [19, 20]. This requires simultaneous consideration of both LG variables and lattice dynamics [21, 22]. For Li_xTiS_2, the staging is suppressed [23], but X-ray measurements [24] and ab initio calculations [26] indicate substantial host distortion [23] around intercalation sites and a uniform expansion of the host lattice along its *c*-axis. It is shown [27] that such an expansion induces a concentration- and distance-independent attraction between the intercalants. A general thermo-mechanical theory of the stress–composition interaction is developed by Larche and Cahn [28]. This implies the existence of a coupling between the elastic properties of the host material and the structure and/or the dynamics associated with the guest species. In other words, the configurational and structural transitions should be considered as coupled. In our previous papers, we have investigated such a coupling for two-dimensional [30–32] and, semiempirically, for three-dimensional systems [33–36]. In application to the intercalation, the theory agrees well with experimental data on layered Li_xTiS_2 and crystalline Li_xWO_3 and Na_xWO_3 compounds at equilibrium conditions.

In this paper, we present a short review of the theoretical methods which has been introduced for a description of the configurational and the structural transitions. The discussion is based on our recent results and their applications to real experiments. The main point is to underline the role of the coupling between the insertion statistics and the host elastic response.

Thermodynamics and kinetics of the insertion

The change in the free energy F of an insertion compound due to the changes in its concentration x inside a host and temperature T is given by

$$dF = -SdT + N\mu_G dx \tag{1}$$

where S is the entropy, N is the total number of available host sites, and $\mu_G=\mu$ is the guest chemical or electrochemical potential. The latter gives a deviation of the electrode potential V from its standard value E_0, $\mu = -eV - E_0$. For the intercalation of neutral species, μ is related to the guest pressure (e.g., hydrogen in metals). Therefore, if the temperature is fixed, then the insertion isotherm, $\mu(x)$, determines all the relevant equilibrium quantities. In particular, the differential capacity $C(x)$ (in fact, the electrode capacity) is determined by an analog of the isothermal compressibility

$$C(x) = \left(\frac{\partial x}{\partial \mu}\right)_T \tag{2}$$

which is a measure of the fluctuation of an actual composition about its average value. If an intercalation process is supplemented by a phase transition, then $C(x)$ is expected to exhibit sharp peaks at the transition concentrations. If $Q(t)$ is the guest charge inside the matrix as a function of time t, then the charge (or discharge) current I is given by

$$I = \frac{dQ}{dt} = \frac{dQ}{d\mu}\frac{d\mu}{dt} = Q_0\frac{dx}{d\mu}\frac{dV}{dt} = Q_0 C(x)\frac{dV}{dt} \tag{3}$$

where Q_0 is the charge at $x=1$. At a constant voltage rate $dV/dt = const$ (the so-called linear sweep voltammogram) the current is modulated by the $C(x)$ behavior.

In many cases, there are two mobile species inside host matrices: the host electrons and the guest particles. Therefore, the transport is characterized by their flux densities J_e and J_G, related to the gradients of the corresponding chemical (or electrochemical) potentials μ_e and μ_G.

$$J_e = L_{ee}\nabla\mu_e + L_{eG}\nabla\mu_G \tag{4}$$

$$J_G = L_{GG}\nabla\mu_G + L_{Ge}\nabla\mu_e \tag{5}$$

where L_{ab} are phenomenological transport coefficients, which are scalar quantities if the host is spatially isotropic. In matrices with a metallic conductivity, the electrons are much more mobile than the guest species. Due to this, the guest ionic charge is compensated by the electrons. For the same reason, the electrons reach a uniform (equilibrium) distribution much faster than the intercalants ($\nabla\mu_e=0$ on the time scale when $\nabla\mu_G\neq 0$). In addition, usually, $L_{GG}>>L_{eG}$ [1]. Therefore, one may focus on the guest flux

$$J = -M(x)x\nabla\mu = -D(x)\nabla x \tag{6}$$

where $M(x)$ is the mobility coefficient that must contain a blocking factor $M(x) = M_0(1-x)$, determining the concentration-dependent chemical (or collective) diffusion coefficient $D(x)$

$$D(x) = M_0 x(1-x)\frac{\partial\mu}{\partial x} \tag{7}$$

Under the assumptions above, the intercalant transport is described by the diffusion equation with an effective diffusion coefficient $D(x)$. The latter requires information on the intercalation isotherm $\mu(x)$. Then, based on the equilibrium properties, at a given concentration gradient, one, at least in principle, can solve the kinetic problem.

Note that such a simple scheme should be modified when the host decreases its conductivity upon intercalation (for instance, Li_xWO_3). Then, the electronic impact should be taken into account. Also, we do not consider other driving forces, like external field or stress gradients, assuming that the guest concentration, x, is the only independent variable. And finally, near the phase coexistence (e.g., staging) a system becomes non-uniform because of the phase boundaries. Then, the formulation of the kinetic problem must be coherent with the theory of critical phenomena (see [29] for a recent review).

Configurational transitions

Lattice gas description

A distribution of the intercalants on the host sites is given by a set of occupation numbers $\{t_i\}$, with $t_i=0$ or $t_i=1$. The guest subsystem is characterized by the chemical potential μ and the nearest-neighbor interaction parameter W (at equilibrium positions). For the electrochemical insertion, chemical potential μ gives a deviation of the electrode potential $-eV$ from its standard value E_0. In this way, an arrangement of the intercalants on a rigid host lattice is governed by the LG Hamiltonian

$$H_G = W\sum_{ij} t_i t_j - \mu\sum_i t_i \tag{8}$$

that describes the configurational transitions of the intercalated species. These could be the droplet formation for attractive interactions ($W<0$) or the order–disorder transition for repulsive interactions ($W>0$). In the latter case, one introduces the sublattice concentrations as appropriate for the symmetry of a given system. Calculating the free energy (or the grand potential) within the mean field approximation, one obtains the well-known relation [1, 4] for the chemical potential at equilibrium

$$\mu_0(x) = -eV - E_0 = qWx + \frac{1}{\beta}\ln\left(\frac{x}{1-x}\right) \tag{9}$$

where q is the coordination number of the host lattice and $\beta=1/kT$.

The permselectivity effect

The approach above describes the intercalation as a simple deposition process of neutral particles in the host lattice. In reality, one deals with Li^+ ions that are screened by the host electrons. Nevertheless, we do not have direct evidence for a perfect neutralization of Li^+ charge by the electronic species. In addition, the ions appear in the host after a dissociation of Li-bearing salt, with the negative ions being strongly excluded from the host matrix. Therefore, for electrochemical insertion, we have to keep in mind that the intercalant transport into the host is due to the electronic and ionic exchange across the (current collector)/(intercalation electrode) and the (intercalation electrode)/(solution) interfaces. In this case, we have to discuss the real situation with a system composed of counterions and electrons. And, we have to take into account the thermodynamic equilibrium, the overall electroneutrality, and the exclusion of one ionic component from the host (it is costly because of Coulombic attraction between coions and counterions)—the so-called permselectivity effect. A detailed calculation of the free energy may be found in [9]. We follow this paper in our derivation. It is known [9] that the interaction between intercalants, as well as their entropy, is modified if compared with the LG:

$$\frac{\beta F}{N} = \left(\frac{\beta F}{N}\right)_{LG} - q\beta W/2 + x[\ln(2x) - 1] \tag{10}$$

where F_{LG} is the LG free energy corresponding to a deposition of ions without any constraint. In addition, we have an interaction-like term $q\beta W^* x/2$ and an entropic impact coming from neutralizing electrons and exclusion of negative ions. Note that these corrections are "irreversible", that is, there are no switching parameters in front, which could turn them off at some nontrivial extreme cases. This reflects a principal difference between a constrained insertion and the LG deposition. The resulting interaction part of the free

energy is now $q\beta W'(x^2-x)/2$, which is the local site–site interaction (quadratic term) corrected by a linear term. The latter accounts for a partial neutralization of the direct repulsive interaction between Li^+ ions. Together with the entropic term, the problem becomes asymmetrical with respect to $x=1/2$. Such an asymmetry is clearly observed in experiments (e.g., voltage vs concentration curves). This gives the chemical potential

$$\overline{\mu}_0(x) = qW'\left(x\frac{1}{2}\right) + \frac{1}{\beta}\ln\left(\frac{2x^2}{1-x}\right) \tag{11}$$

which is not symmetric with respect to $x=1/2$. Such a breaking of the hole–particle symmetry is typical for the experimental voltage-concentration dependencies.

Structural transitions

During the intercalation, almost all host matrices exhibit a composition-dependent unit cell volume. This occurs in the course of various restructuring processes, like a simple volume expansion, staging [41], or the host lattice reconstruction. For layered compounds, the main contribution to the volume change comes from the *c*-axis expansion. This anisotropy allowed to introduce a set of simple models describing the concentration-dependent layer spacing $d(x)$. The latter is normalized such that $d(0)=0$ and $d(1)=1$. The simplest form $d(x)=x$ corresponds to the Vegard law. In application to Li_xTiS_2, a rigid-layer model has been introduced [21, 22]. In this model, undeformable (rigid) layers are coupled by springs, whose constants correspond to the host–host and the host–guest interactions. This approach gives

$$d(x) = \frac{x}{x + a(1-x)} \tag{12}$$

which reduces to the Vegard law when the spring constant combination $a\rightarrow 1$. The role of the in-plane deformation has been discussed within the layer rigidity model [38] which gives

$$d(x) = 1 - (1-x)^P \tag{13}$$

where P is the layer rigidity parameter. The latter model has been shown [38] to give better fits to experimental data than the former one. Nevertheless, in application to Li_xTiS_2, both are only qualitatively correct. The experimental $d(x)$ curves are of a sigmoidal shape with inflection points suggesting a hidden tendency [35] towards the staging [19, 20]. The *k*-stage ordering is connected with a periodic (along the *c*-axis) sequence of *k* host layers and one intercalant layer. In this case, the unit cell volume exhibits a very sharp increase at compositions corresponding to the change of the stage state (for instance, when one goes from *k*-stage to *k*−1-stage).

The approaches outlined above describe the concentration-dependence of the unit cell volume. But, the influence of this effect on the insertion thermodynamics was not analyzed. For that reason, in the next section, we discuss such a coupling.

Configurational–structural coupling

The main idea of the following discussion is to emphasize that the structural and the configurational transitions are not independent [33, 35].

The host material is described as a three-dimensional lattice of adsorbing sites with their positions given by set vectors (r_i). Due to the elastic properties of the real host, each site (for instance, an interstitial site) of this "auxiliary" lattice may deviate from its equilibrium position r_i^0, such that we deal with the displacements $u_i = r_i - r_i^0$. Therefore, the host properties are described by the Hamiltonian $H_H[\{u_i\}]$. Note, however, that a connection between the elastic properties of the real matrix and those of the adsorbing lattice is not straightforward [33, 34]. Anyway, in the absence of the guest species, the host does not undergo any remarkable transformation, so that H_H is related to "regular" host properties (e.g., thermal vibration).

The coupling between the host and the guest is given by Hamiltonian $H_C[\{u_i\},\{t_i\}]$ which takes into account a dependence of the binding energy on the site displacement and also the pairwise interaction between the guest particles through the host lattice. The overall Hamiltonian is now written as

$$H = H_H[\{u_i\}] + H_G[\{t_i\}] + H_C[\{u_i\},\{t_i\}] \tag{14}$$

The free energy F corresponding to the above Hamiltonian is given by

$$F = F_H + F_G(x) + F_C(x) \tag{15}$$

where x is the intercalant concentration. Here, F_H is the host free energy in the absence of intercalation; F_G is the guest free energy in a case of the rigid host lattice. This is the configurational part corresponding to the LG description and giving the chemical potential $\mu_0(x)$ (see Eq. 9).

The coupling term can be estimated within a perturbation scheme [30] implying that

$$\beta F_C = -\ln\left(\left\langle\left\langle e^{-\beta HC}\right\rangle_{(u_i)}\right\rangle_{(t_i)}\right) \tag{16}$$

requires the averaging over the displacements and the occupation numbers, calculated with the reference terms H_H and H_G. In fact, this is an infinite series including the correlations of all orders in the reference state. The main problem is to specify $H_C[\{u_i\},\{t_i\}]$ coherently with the host symmetry and elastic properties. It is known that real host

materials have rather complicated elastic properties (e.g., a strong anisotropy). Therefore, only some simplified model calculations are expected to give tractable results. On the other hand, such predictions (e.g., the rigid plane model [22]) do not exhibit quantitative agreement with experimental data. Approximate perturbative scheme developed previously [33, 34] has shown that the coupling term concerns with a concentration-dependence of the host response to the intercalation. This includes two effects. First is a renormalization [1, 37] of the pair interaction between the intercalants inside the matrix. The second is a change of the host volume upon insertion of the guest species. Depending on the host nature, a stress field may result if the lattice is not totally free to relax. In this situation, it seems reasonable to estimate the coupling term based on the continuum theory of elasticity with the concentration-dependent stress and strain fields. Then, the host–guest free energy is a sum of the lattice gas and elastic part

$$F(x) = F_{LG}(x) + F_{el}(x) \tag{17}$$

where $F_{LG}(x)$ is the configurational (lattice gas) part, in which the pairwise interaction is renormalized [1] due to the interaction through the matrix. This gives the chemical potential $\mu_0(x)$ (see Eq. 9) with a new interaction constant W. The elastic part is approximated by the free energy of a strained isotropic body under a loading stress $\sigma(x)$. Since the strain is assumed to be purely dilatational, we operate with traces ε and σ of the corresponding tensors.

$$F_{el}(x) = \frac{\Lambda}{2}\varepsilon(x)^2 - \sigma(x)\varepsilon(x) \tag{18}$$

with Λ being the effective elastic constant, independent of the concentration. The total stress $S=S(x)$ is given by

$$S(x) = \frac{dF_{el}}{d\varepsilon(x)} = \Lambda\varepsilon(x) - \sigma(x) \tag{19}$$

Therefore, we have two stress contributions. The internal, or self-stress $\Lambda\varepsilon(x)$ corresponds to the host reaction to the guest insertion. The second term $\sigma(x)$ describes a loading procedure that may include the sample clamping or other effects which are not directly related to the strain. It is important that, in general, $\sigma(x)$ is a function of x (not a function of $\varepsilon(x)$). For instance, if the sample is clamped such that $\varepsilon(x)=0$, then we have a stress accumulation proportional to the concentration $\sigma(x) \propto x$.

Equilibrium properties

The guest chemical potential $\mu(x)$ is given by the concentration derivative of the total free energy.

$$\mu(x) = \mu_0(x) + S(x)\frac{d\varepsilon(x)}{dx} - \frac{d\sigma(x)}{dx}\varepsilon(x) \tag{20}$$

Here, the second term involves the so-called chemical expansion coefficient $d\varepsilon(x)/dx$, while the last term is associated with the loading path. It is seen that the intercalation level depends on interplay of the internal stress and the loading stress. The latter could be small, but its concentration derivative is not necessary small, so that the loading path can have serious consequences [12]. In particular, for a given material (Λ) and a suitable loading path $\sigma(x)$, one can have a cancelation of the last two terms in Eq. 20 in a given domain of x. This explains why, in some cases, the purely configurational description ($\mu(x)=\mu_0(x)$) works well. If the host–guest system forms a solid solution, then the guest partial molar volume $V_m(x)$ is related to the total volume $V(x) = xV_m(x) + V_0$, where V_0 is the initial host volume (at $x=0$). On the other hand, the strain is also related to the volume variation $\varepsilon(x) = (V(x) - V_0)/V_0 = xV_m(x)/V_0$.

If the loading is composition-independent $\sigma(x)=\sigma$ and the sample volume changes linearly ($V_m=const$, $\varepsilon(x)=xV_m/V_0$, like in the PdH_x α-phase), then we recover the well-known result [15]

$$\mu(x) = \mu_0(x) - (\sigma - \Lambda x V_m/V_0)V_m/V_0 \tag{21}$$

.

In our previous works [33, 34], we have analyzed another extreme case of vanishing total stress $S(x)\to 0$ and the loading stress proportional to the concentration $\sigma(x)=\sigma_0 x$. Then

$$\mu(x) = \mu_0(x) - \gamma p(x) \tag{22}$$

where $\gamma = (V(1) - \mathrm{V}_0)/\mathrm{V}_0\sigma_0$ and $p(x) = (V(x) - V_0)/(V(1) - V_0) = \varepsilon(x)V_0/(V(1) - V_0)$. Note, however that, for $\Lambda=const$, the above result is valid only for a linear behavior of $p(x)=px$, while is an approximation for an arbitrary $p(x)$. In reality, the elastic constants depend on the concentration, for instance the bulk modulus of Pd is reduced [14] up to 20% due to the hydrogen sorption. Thus, one can easily imagine a situation when $\Lambda(x)\varepsilon(x)\approx\sigma(x)$ and then the approximation (22) is applicable for a nonlinear $p(x)$. In general, for a non-Vegard's behavior and the linear loading $\sigma(x)=\sigma_0 x$, we deal with a modified LG (MLG) description.

$$\mu(x) = \mu_0(x) + \left[\overline{\Lambda}p(x) - \gamma x\right]\frac{dp(x)}{dx} - \gamma p(x) \tag{23}$$

where $\overline{\Lambda} = \Lambda\gamma^2/\sigma_0^2$.

The strain can be measured as a volume dilatation or as a change of the interlayer spacing during the transitions between different phases (staging in graphite, restructuring in Li_xWO_3, $\alpha-\beta$ transition in PdH_x, etc). In any case, the lattice parameters do not obey [38] the linear Vegard's law, exhibiting a sharp change near the transition compositions

x_n^0. This is described by the following approximation (an absolute value is considered).

$$p(x) = \frac{1}{2}\left[1 + \sum_n p_n \tanh\left[\alpha_n\left(x - x_n^0\right)\right]\right] \quad (24)$$

where n counts the number of phase boundaries. In Li_xWO_3, n=1,2 corresponds to monoclinic–tetragonal and tetragonal–cubic transitions, respectively. Although for Li_xTiS_2 the staging is suppressed [23], the interlayer spacing exhibits a non-Vegard's variation and an inflection point near $x \approx 0.09$ becomes more pronounced with decreasing temperature [7]. This implies a hidden tendency towards the staging [35] (with n=1,2 marking the boundaries), which becomes the real staging when, for instance, *Li* is substituted by *Ag* ions [25].

In Fig. 1, the normalized interlayer spacing $p(x)$ Eq. 24 is displayed as a function of *Li* concentration in TiS_2 matrix. The set of rigidity parameters, α_n, controls a local slope, and p_n, are the weights corresponding to each phase, such that $\Sigma_n p_n = 1$. This is consistent with experimental observations [6] indicating that the structures are not completely pure, but contain some features that indicate a mixing of phases. The present form of $p(x)$ corresponds to continuous structural transitions, but can be easily modified to take into account the jump-like behavior (like for the staging [1]).

Based on the fitting for $p(x)$, we obtain the isotherm and the capacity curve, which are plotted in Fig. 2 as functions of the *Li* composition. It is seen that the purely configurational behavior (pure LG, dotted lines) takes place only at low (or high) intercalant concentrations. At intermediate x, the structural changes ($p(x)$) are important. For instance, the hole–particle symmetry of the LG description is broken by the elastic effects. It is seen that the MLG scheme (solid line), taking into account the matrix response, allows us to reproduce the characteristic capacity peak near x=0.27. As mentioned above, the peak is often associated with a hidden tendency of the TiS_2 matrix towards the staging. Anyway, it is clear that the peak position strongly correlates with the inflection point of the $p(x)$ curve, indicating that the increase in the capacity is due to the peculiarity of the matrix response.

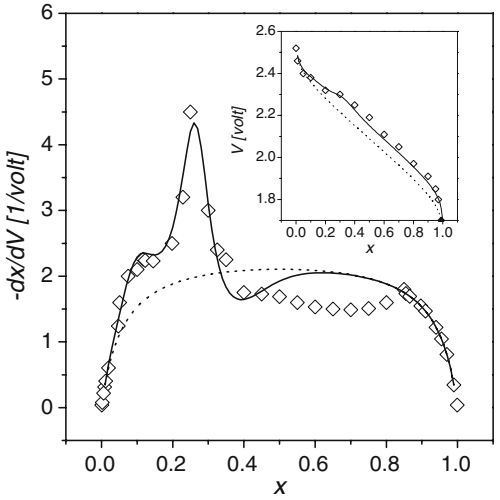

Fig. 2 Voltage (*inset*) and capacity for Li_xTiS_2 as functions of *Li* concentration. The *symbols* correspond to the experimental data [7]. The *dotted lines* correspond to the pure LG description, and the *solid lines* correspond to the MLG approach. The parameters: $\beta\gamma$=2, $\beta\Lambda = 0.4$, βW=2.5, β correspond to room temperature

In Fig. 3, we display the intercalation isotherm (inset) and the capacity curve, comparing them to the experimental data [6] for Li_xWO_3. The fitting Eq. 23 is performed assuming that the effective pair interaction inside the matrix is repulsive for any x. The curve modulation results from the strain behavior $p(x)$, associated with the volume

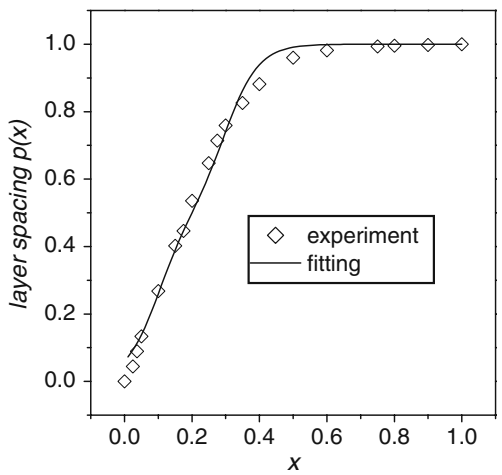

Fig. 1 Normalized layer spacing $p(x)$ as a function of *Li* concentration x. The *symbols* correspond to the experimental data [21]. The parameters: $p_1 = p_2 = 1/2$, α_1=10, α_2=12, $x_1^0 = 0.09$, $x_2^0 = 0.27$

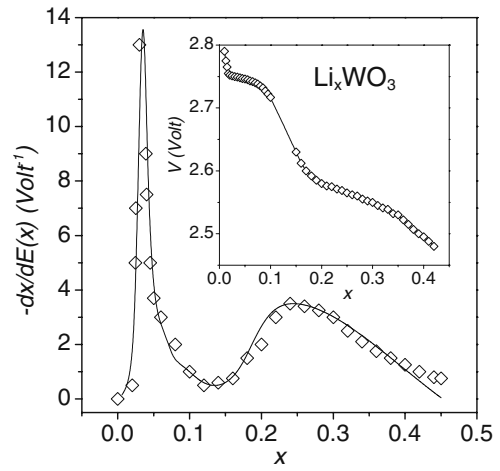

Fig. 3 Differential capacity and the voltage (*inset*) for crystalline Li_xWO_3. The symbols correspond to the experimental data [6]. The parameters p_1=0.7, p_2=0.3, $\alpha_1 = \alpha_2 = 15$, $x_1^0 = 0.05$, $x_2^0 = 0.27$, $\beta\gamma$=1.8, $\beta\Lambda = 0.01$, βW=2.2

dilatation. As is discussed previously [34], the peculiarities (inflection points and the peaks in $C(x)=dx/d\mu$) mark the boundary between different host symmetries. From the experimental point of view, the peak height is usually associated with transition sharpness.

Note, however, that the experimental dependencies are usually smoothed due to a finite concentration resolution. Then, it is difficult to distinguish between the stepwise variation and a sharp (but continuous) transition. For that reason, the criticality criteria, determined on the ground of rigorous statistical mechanical arguments ($\mu(x)$ loops or a divergent capacity $C(x)$), only approximately conform to the experimental data. Therefore, the critical behavior of the model itself should be studied separately.

Diffusion

Starting from (20) and (7), we obtain the chemical diffusion coefficient (CDC) as

$$D(x) = D_0(x) + D_{el}(x) \tag{25}$$

where the first term is the standard LG part $D_0(x) = D_0 x(1-x)\frac{\partial \mu_0}{\partial x}$ and the elastic contribution is given by

$$\frac{D_{el}}{B(x)} = S\frac{d^2\varepsilon}{dx^2} + \Lambda\left(\frac{d\varepsilon}{dx}\right)^2 - 2\frac{d\varepsilon}{dx}\frac{d\sigma}{dx} - \frac{d^2\sigma}{dx^2}\varepsilon \tag{26}$$

with $B(x) = D_0 x(1-x)$. The CDC involves several competing factors (strains, stresses, and their concentration derivatives). In general, it is not trivial to see whether D increases or decreases with x. The situation is even more complicated for systems in which the lattice spacing does not obey the linear Vegard's law, but has inflection points separating different phases (e.g., staging in graphite or restructuring in Li_xWO_3). Then, the derivatives above may change sign with the concentration. Also, we see again that the loading path has a significant contribution.

For PdH_x (α-phase), we recover the well-known result [14, 15]. The concentration induced internal stress $S_0(x)=\Lambda x V_m/V_0$ increases CDC

$$D = D_0(x) + B(x)A(V_m/V_0)^2, \tag{27}$$

where $D_0(x)$ is the stress-free CDC (it corresponds to $\mu_0(x)$, i.e., the lattice gas description, see above). Note that the non-local stress effects [13, 14], which tend to depress the diffusion, are not discussed here.

Since, according to (7), the diffusion coefficient is just an inverse of $C(x)$, D as a function of x should have minima corresponding to the peaks in the capacity curve [36]. Such a behavior is observed experimentally for Li_xWO_3 [40], Li-graphite [41], and for many other intercalation systems. This is illustrated in Fig. 4 where the concentration-dependence of the diffusion coefficient for crystalline

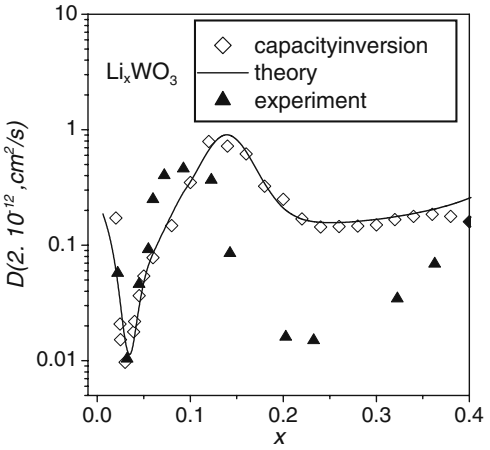

Fig. 4 The chemical diffusion coefficient for crystalline Li_xWO_3. The *symbols* (*up triangles*) correspond to the experimental data [31], obtained from the electrochemical impedance spectroscopy. The theoretical parameters are the same as for the previous figure

Li_xWO_3 is presented. For comparison, the inverse capacitance data are presented. Following the same strategy, from a fitting of the interlayer spacing $p(x)$ for Li-graphite system (Fig. 5), we have calculated the capacitance and then the diffusion coefficient (Fig. 6). The same tendency is clearly observed. Namely, CDC has a set of minima which correspond to the inflection points of $p(x)$ separating different stages. The minima are usually attributed [41] to a clustering tendency near the phase boundaries, induced by an effective attraction between the intercalants through the host lattice. Formally, the elastic part of the chemical potential (20) can be combined with the interaction term of LG part to form the effective interaction [33, 34] $\Phi(x) = qWx - \gamma p(x)$ which may become attractive (even for $W>0$) for concentrations at which the elastic part exhibits strong variations. The latter take place near $x = x_n^0$. Therefore, D should have minima around x_n^0, and the experimental observations

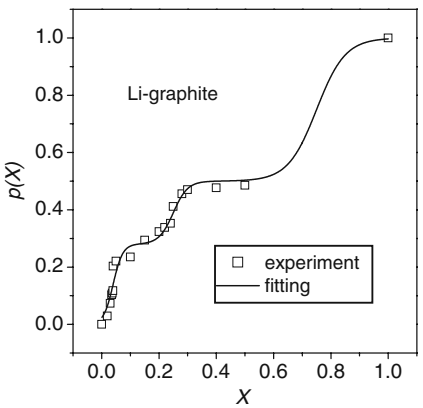

Fig. 5 The average interlayer spacing for Li-graphite. The experimental data are extracted from [12, 13]. The theoretical fitting is performed using Eq. 13 where p_1=0.28, α_1=30, $x_1^0 = 0.04$, p_2=0.22, α_2=20, $x_2^0 = 0.25$, p_3=0.5, α_3=20, $x_3^0 = 0.75$

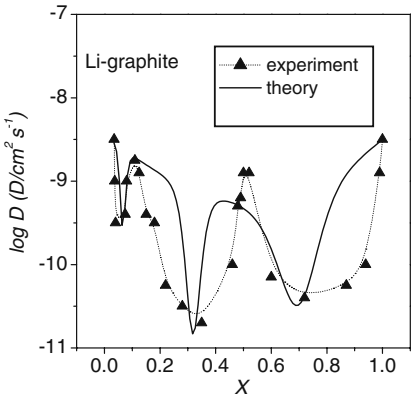

Fig. 6 The chemical diffusion coefficient for Li-graphite. The experimental data are extracted from [33]. The fitting is done using Eqs. 12, 18, and 19 where $\beta cW=-0.1$, $\gamma=0.5$, $\Lambda=0.1$. The parameters for $p(x)$ are the same as in the previous figure

confirm this conjecture. The present approach allows us to separate the factors which contribute to such a behavior, suggesting that we deal with interplay of the renormalized pairwise interaction and the cooperative effects due to the strain and stress fields.

Concerning a quantitative comparison with the experimental data, our estimations for Li_xWO_3 and Li-graphite suggest that the present theory works well around the transition compositions x_n^0 but overestimates the diffusion coefficient by several orders of magnitude at $x \neq x_n^0$. This seems surprising since the equilibrium characteristics are described correctly at any composition. There could be several reasons for such a discrepancy. First of all, the intercalation compound usually changes their electronic conductivity [39] upon the guest insertion. Then the one-component description should be extended to include this effect. On the other hand, the composition-dependence of CDC is usually deduced from experimental measurements [e.g., electrochemical impedance spectroscopy (EIS) or potentiostatic intermittent titration (PITT)] employing a model whose consistency with our approach remains to be investigated. In addition, these two experimental methods give different estimations [41] of the CDC.

Disordered host matrices

As have been mentioned above, insertion processes have received considerable interest because of their applications in a variety of technologically important domains, e.g., storage devices [2, 44], high capacity batteries, electrochromic devices, solar cells, etc. (see [1] for a review). These materials are usually produced by insertion or doping of a host matrix by neutral or charged guest species. Typical examples are the intercalation compounds or conducting polymers. In many cases (e.g., amorphous/porous materials or polymer films), the host matrix is spatially disordered. This has some advantages [45] (e.g., higher capacity) in comparison to crystalline hosts. In particular, this allows one to avoid the macroscopic insertion-induced phase transformations, such as restructuring (crystalline WO_3) or staging (graphite). In its turn, this broadens the voltage and composition ranges where a stable cycling can be maintained.

From a theoretical point of view, the host disorder is usually described by a distribution of some relevant quantity, such as pore sizes or site energies [6, 46, 47]. Then, the insertion isotherm is represented as an average over the host fluctuations. Despite a considerable progress [46] in the field, the consequences of the disordered host morphology are still poorly understood. In particular, recent theoretical studies [48, 49] of adsorption into disordered porous media suggest that, because of the host disorder, the adsorption thermodynamics might depend on a driving path (e.g., controlled injections of prescribed portions or an equilibrium with a bulk reservoir). In the context of intercalation processes, this means that different electrochemical methods (e.g., chronopotentiometry and voltammetry) could give different results. Therefore, analyzing a system by different techniques could help in the characterization of the host morphology.

The problem is complicated by the structural changes occurring upon insertion [50, 51] or intercalation [52, 53]. In many cases, mechanical strain generated in the intercalation/deintercalation cycles induce structural as well as volume changes in the electrode material, leading to fracturing, cracking, and even crumbling, and thereby to electrode irreversibility upon cycling. One of the most challenging issues in the development of devices based on lithium intercalation materials is the control over structural changes and deformations produced by lithium insertion/removal. These can be manifested as spatially distributed internal distortions which lead either to topotactic insertion [45] or even to macroscopic (up to 10%) volume dilatations [53, 54]. The latter are easily detectable (e.g., by optical profilometry [53]), while the internal distortions are rather difficult to control. For this reason, quite often, the internal host structure remains poorly characterized. On the other hand, a coupling between the insertion and the dilatation modes has been shown [55, 56] to be responsible for well-pronounced thermodynamic features. Even in the absence of detectable volume variations, the internal host distortion should contribute [57] a fluctuational term to the insertion thermodynamics. Therefore, one should be able (at least in principle) to distinguish these two effects.

In the absence of detailed microscopic information, one has to analyze the underlying physics directly from the experimental data and a plausible insertion model. The aim of this work is to develop a holistic theoretical scheme, able

to extract from an experimental isotherm, $\mu_b(x)$, the volume variation and the internal distortion traces. This would allow us to analyze their impacts to the observed behavior. With this purpose, we combine the distortive lattice gas model that has been successfully applied [35] to a description of volume dilatation in ordered intercalation compounds with the maximum information entropy approach [58]. The latter is an inductive inference method which is quite efficient [49] in estimating the host disorder from the experimental isotherm data. Then, we test our predictions, trying to explain some puzzling points in the recent experimental results [53].

Overview of experimental results

Recent experiments [53, 54] on amorphous Li_xWO_3 compounds reveal that the insertion thermodynamics differs remarkably from the lattice gas picture, conventionally used for the description of intercalation into rigid crystalline matrices. In particular, the isotherms and the capacitance curves have been shown to involve power-law dependencies on the guest concentration, x [53].

$$\mu_b = E_0 + (1+\eta)Gx^{\eta} + \frac{1}{\beta}\ln\left(\frac{x}{1-x}\right). \tag{28}$$

The capacitance $C_\mu \propto [\partial\mu_b/\partial x]^{-1}$ that follows from Eq. 28 has been found in an excellent agreement with the experimental data. This is demonstrated in Fig. 1 for the case of lithium intercalation into amorphous WO_3 films of different thickness. Therefore, in what follows this relation Eq. 28 will be considered as an experimental fact. Here, G was interpreted as a host–guest interaction parameter. However, it has been found to depend on the host film thickness. For the thinnest (100 nm) film, the intercalant–host interaction term G is not detectable ($G\approx 0$) so that the system behaves like an ideal noninteracting lattice gas in which entropic contributions play the determining role. As the thickness increases, G becomes larger, attaining values around 350 meV for thicker (400 nm) films, what modifies the asymptotic behavior of the chemical capacitance. The exponent of the intercalant–host interaction term has been found to be around $\eta\approx 0.5$. Such a variation of the host–guest interaction parameter is difficult to understand because the interaction between the two subsystems is essentially determined by their chemical nature. Variation of G with the thickness is accompanied by specific volume changes of the host matrix [53]. The relative volume changes at $x=0.4$ of a 200 nm amorphous $LixWO_3$ film are shown to yield a highly rough surface in the intercalated part. All films showed relative volume changes near 10% on average, except for the 100 nm-thick samples which presented no expansion at all, in agreement with the results of electrochemical measurements ($G\approx 0$).

Therefore, the experiments [53, 54] provide an evidence for the significant role played by the film volume change and the surface roughness in the underlying intercalation thermodynamics (cell voltage variation with the guest composition). Importantly, these results make apparent the occurrence of some sort of thickness effects which are poorly understood.

Volume variations

The host volume variations can be taken into account in the framework of the lattice gas model combined with the continuum elasticity theory. This leads to the following isotherm [35]

$$\mu = \mu_0(x) + S(x)\frac{d\varepsilon(x)}{dx} - \frac{d\sigma(x)}{dx}\varepsilon(x) \tag{29}$$

where $\beta\mu_0(x) = \beta E_0 + \ln(x/(1-x))$ is the standard lattice gas part without the guest interaction, and $S(x) = \Lambda\varepsilon(x) - \sigma(x)$ is the concentration-dependent total stress. The latter involves the external (loading) stress $\sigma(x)$ and the internal stress $\Lambda\epsilon(x)$. Here, Λ is the elastic constant related to the Young modulus, and $\epsilon(x)$ is the strain which results from the changes in the host volume $V(x)$. In the case of unclamped matrices, we may neglect the loading contribution, arriving at

$$\mu = \mu_0(x) + \Lambda\delta^2 p(x)\frac{dp(x)}{dx}, \tag{30}$$

where $\delta = [V(1) - V(0)]/V(0)$ is the relative volume variation and $p(x) = [V(x) - V(0)]/[V(1) - V(0)]$ is the modulating function with $p(0)=0$ and $p(1)=1$. Identifying the elastic part in Eq. 30 with the power-law term in Eq. 28 and solving with respect to $p(x)$ one gets a sublinear (recall that $\eta\approx 0.5$) modulating function [53]

$$p(x) = x^{(1+\eta)/2} \tag{31}$$

and the coupling of the empirical parameter G and the relative volume expansion

$$\delta = \left(\frac{G}{\Lambda}\right)^{1/2}. \tag{32}$$

It has been shown [53] that the capacitance derived from Eq. 30 predicts the film volume expansion around 10% (on average) at the intercalation level $x\approx 0.4$. These volume changes have been directly observed by optical profilometry for the film thickness≥200 nm. Nevertheless, these results do not allow accounting for the threshold-like behavior [53] of the volume expansion with the film thickness.

Internal distortions

The experimental results [53] clearly indicate that the matrix volume variation is accompanied by an extensive

roughening of the surface in the intercalated region. Based on this, we suppose that, in addition to the dilatation, the host undergoes some internal distortions. These are related to an adjustment of the host structure allowing for a more efficient accommodation. This can be taken into account as a correction φ to the host–guest interaction, changing the insertion energetic cost

$$\mu(x|\varphi) = \varphi + \mu_0(x) + \Lambda\delta^2 p(x)\frac{dp(x)}{dx}, \tag{33}$$

where φ is a fluctuating quantity distributed according to some probability density $f(\varphi)$. The latter is unknown; the only available experimental evidence we have is the isotherm (28). Therefore, we infer the distribution using the maximum information entropy approach [49, 58, 59]. The procedure consists in maximizing the Shannon entropy measure

$$H = -\int d\varphi f(\varphi)\ln f(\varphi) \tag{34}$$

under the constraint that the average $\overline{\mu(\varphi)}$ reproduces the experimental data (28)

$$\mu_b = \overline{\mu(x|\varphi)} = \int d\varphi f(\varphi)\mu(x|\varphi). \tag{35}$$

This gives the following concentration-dependent distribution

$$f(\varphi|x) = \frac{\exp[\lambda(x)\mu(x|\varphi)]}{\int d\varphi \exp[\lambda(x)\mu(x|\varphi)]}, \tag{36}$$

where the Lagrange multiplier $\lambda(x)$ should be found from the constraint (35). This leads to

$$(1+\eta)Gx^{\eta} = \varphi(x) + \Lambda\delta^2 p(x)\frac{dp(x)}{dx}, \tag{37}$$

where $1/\lambda(x) = \varphi(x) = \overline{\varphi}$. It is seen that the power-law term involves a combination of the distortion and the volume dilatation. These effects have been found to depend on the host film thickness [53]. Thus, it is not surprising that the parameter G is also thickness-dependent. On the other hand, Eq. 37 determines the dilatation and the internal distortion impacts to the observed thermodynamics. Having a plausible estimation for one of these ingredients allows us to estimate the other.

Analysis of experimental data

In what follows, we will try to see to what extent interplay of the host distortion and dilatation is able to explain the behavior observed in amorphous Li_xWO_3 films.

Note that the last term in Eq. 37 includes not only the dilatation magnitude $\delta p(x)$ but also the dilatation rate $R(x)=dp(x)/dx$. Even if (at some point $x=x_0$) the distortion contributions $\varphi_1(x_0)$, $\varphi_2(x_0)$ and the volume dilatations $p_1(x_0)$, $p_2(x_0)$ are the same for two films of different thickness, their isotherms could be distinguished by different rates $R_1(x_0)=R_2(x_0)$. This gives an idea on why the host films with almost the same dilatation magnitudes (as in the case of 300 and 400 nm films at $x_0=0.4$) exhibit different electrochemical responses. Therefore, measuring simultaneously the isotherm and the concentration-dependent volume variations one can get some information on the internal distortions.

On the other hand, having an estimation of the internal host morphology, one can predict the volume variation. In particular, the recent analysis [54] of the jump diffusion coefficient reveals a power-law dependence of the hoping rate on the concentration. Based on this, we may suppose $\varphi(x)=-Kx^q$, with K being an effective distortion coefficient. Then, Eq. 37 can be solved with respect to $p(x)$. This leads to

$$p(x) = \left[\frac{G}{\Lambda\delta^2}x^{\eta+1} + \frac{K}{\Lambda\delta^2(q+1)}x^{q+1}\right]^{1/2} \tag{38}$$

In order to satisfy the condition $p(1)=1$, the following relation should hold

$$\frac{G}{\Lambda\delta^2} + \frac{K}{\Lambda\delta^2(q+1)} = 1. \tag{39}$$

This allows us to estimate the relative host dilatation at $x=1$

$$\delta = \left(\frac{G}{\Lambda} + \frac{K}{\Lambda(q+1)}\right)^{1/2}. \tag{40}$$

We thus see that, even for $G\approx 0$ (as in the case of 100 nm films), the dilatation does not vanish because of the distortion contribution. From Eq. 39, one can see that $G=0$ corresponds to a subtle relation $K = \Lambda\delta^2(q+1)$ between the dilatation and the internal distortion. The latter is probably rather small for thin films, as this follows from the relatively low surface roughness in comparison to that for the thicker films [53]. For this reason, in agreement with the experimental observations, the volume expansion could be undetectable. On the other hand, the host has been found to undergo irreversible transformations at $x>0.6$. For this reason, the experimental magnitude of δ is not available. The only information at hand is the volume dilatation $\delta\cdot p(x=0.4)$.

Therefore, we have to analyze the volume variation as a function of the concentration. Combining Eqs. 38 and 39, we arrive at

$$p(x) = \left[(1-B)x^{\eta+1} + Bx^{q+1}\right]^{1/2}, \tag{41}$$

where $B = K/\left[\Lambda\delta^2(q+1)\right]$ is a parameter measuring the relative impact of the distortion and the volume variation

effects. Using Eq. 39, we can relate B to the empirical constant $G: B = 1 - G/(\Lambda\delta^2)$. This suggests that $B<1$ and, depending on the other parameters, can even be negative. This, in its turn, means that the distortion coefficient K might change its sign with increasing film thickness (as the parameter G grows). Taking into account that the isotherm (28) is now represented as

$$\mu(x) = \mu_0(x) - Kx^q + \Lambda\delta^2 p(x)\frac{dp(x)}{dx}, \tag{42}$$

we may expect a crossover between two regimes with decreasing host film thickness. For thick films (positive K or B), the internal distortions favor an adjustment of the host geometry, making the insertion less energetically consuming. For thin films (negative K or B), we have to spend energy in order to induce both distortions and volume dilatation (presumably because of a stronger influence of the film support). It is interesting that a quite similar crossover from a quenched to an adsorbate-induced roughness has recently been reported [60] for HCl adsorption on ice films of varying thickness. In the context of the present work, the crossover is due to interplay of the film volume dilatation and the insertion-induced internal distortions. This behavior is illustrated in the Fig. 7, where $p(x)$, given by Eq. 41, is plotted for different values of B. In order to recover the threshold-like variation [53] of the volume with the film thickness, we have to assume that the parameter B changes sign with decreasing thickness. However, this makes the volume variation ill-defined ($p(x)$ $2<0$) in the range of low concentrations. This suggests that, for thin films, another distortion mechanism is probably operating in this domain. Note that the isotherm remains mathematically correct because all our estimations are made under the condition (37) preserving the isotherm shape.

On the other hand, the above artifact may result from the concentration-dependence accepted for $\varphi(x)$. In other words, the power-law shape of the distortion part cannot completely explain the observed electrochemical response.

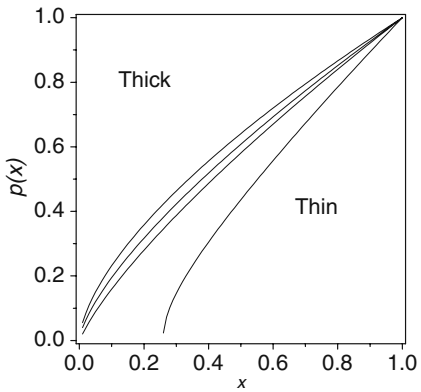

Fig. 7 Modulating function calculated from Eq. 14 at q=0.2, η=0.5, and different B=0.7, 0.2,−0.2,−2 (from *left to right*)

Therefore, making plausible assumptions on $p(x)$ and solving (37) with respect to $\varphi(x)$ seems to be more constructive. In the previous study [35], the following modulating function has been considered

$$p(x) = \frac{1}{2}[1 + \tanh(\Delta[x - x_0])] \tag{43}$$

This generic form mimics a non-Vegard behavior, typical for layered intercalation compounds [35]. As depicted in Fig. 8a, the dilatation is weak at low densities ($x<<x_0$). The most intensive response is at $x\approx x_0$, and then the matrix reaches saturation, corresponding to its mechanical stability limit. Here, Δ is the matrix response constant or dilatation rate, controlling the slope near $x\approx x_0$. Such a threshold behavior of the volume variation with the guest concentration is well-documented for various layered matrices [1, 21] (e.g., Li_xTiS_2). Therefore, accepting that the characteristic concentration x_0 increases with decreasing film thickness, we can explain the observed crossover from thin to thick films. Growth of x_0 with decreasing thickness can be understood as a stronger influence of the film support, such

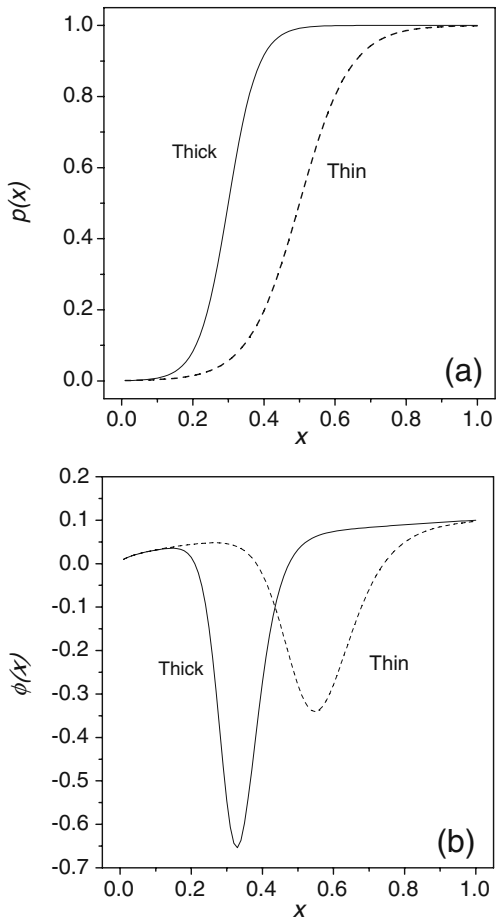

Fig. 8 **a** Modulating functions calculated from Eq. 16 at two characteristic concentrations x_0=0.3 (*solid*) and x_0=0.5 (*dashed*). **b** Corresponding distortion terms $\phi(x)$ calculated from Eq. 10

that higher guest densities are required to induce detectable host dilatations. Having found a reasonable approximation for $p(x)$, we can solve (37) with respect to $\varphi(x)$. This function is plotted in Fig. 8b. It is seen that, in agreement with our previous estimation, the distortion contribution changes its sign in the range of concentrations, close to the threshold point x_0. Therefore, in the low concentration region, the distortion part $\varphi(x)$ for thick and thin films behaves differently. Namely, in the concentration domain where the volume dilatation is negligible, $p(x)\approx 0$ or saturated $dp(x)/dx\approx 0$ the insertion is associated with an additional energy cost $\varphi(x)>0$ to distort the matrix. On the other hand, an increase in the volume allows for an optimization of the internal structure, and this makes the insertion locally more favorable $\varphi(x)<0$.

Conclusion and perspective

Here, we have outlined a theoretical scheme involving a coupling between the electrochemical and elastic properties in the course of various insertion processes. Our approach implies that the main equilibrium and transport features of real intercalation systems (which differ in their microscopic details) can be well-understood in terms of concentration-dependent hydrostatic parts of the stress and strain fields, associated with the internal and loading effects [12]. On the other hand, the approach is flexible enough to incorporate other transport mechanism (migration or electronic mobility effects).

The theory gives a quantitative description of different insertion processes, involving the volume expansion [Li_xTiS_2 (see [33]), $\alpha-PdH_x$] or restructuring (Li_xWO_3). For all these processes, the theory implies a correlation between the intercalation isotherm and a concentration-dependence of the diffusion coefficient. The latter exhibits a set of characteristic minima, related to the boundaries between different phases (like different symmetry phases of Li_xWO_3, $\alpha-\beta$ transition in PdH_x, staging in graphite [41]). However, the experimental dependencies are usually smoothed due to a finite concentration resolution. For that reason, the criticality criteria, determined on the ground of rigorous statistical mechanical arguments (e.g., $D(x)=0$ at the transition concentrations), only approximately conform to the experimental data, exhibiting a sharp (but finite) decrease of D. For a non-Vegard's strain variation the diffusion coefficient is a nonlinear (and nonmonotonic) function of the concentration (26). Therefore, the diffusion equation for the concentration profile would be strongly nonlinear. Then, one can expect a rather complicated space–time variation of the guest density, including, for instance, oscillations [12] and other nonlinear effects. Our results may have implication in various domains related to the insertion process, like hydrogen sorption [2], electrochemical intercalation, impurities in alloys, layered superconductors [3], volume transitions in hydrated gels [43], etc.

Nevertheless, the magnitude of the chemical diffusion coefficient is overestimated even if the equilibrium capacitance is described with a rather good accuracy. This fact makes us to analyze what kind of information is available from the experiments (usually EIS) and which theoretical approaches are required for recovering the experimental results. The EIS method consists in applying a small amplitude overvoltage $E(t)$ oscillating with the frequency ω and measuring the impedance [41, 42] $Z(i\omega)$. The so-called Warburg impedance

$$Z(i\omega) \propto (i\omega)^{-1/2} \tag{44}$$

is associated with the occurrence of a diffusion-controlled process which can be understood in terms of the usual Fickian relation between the flux $J(r)$ and the concentration gradient $J=-D\nabla x(r)$. Strictly speaking, such a relation is valid only for small x when the diffusion coefficient D is composition-independent (see Eq. 6). This constitutive relation is supplemented by the conservation law relating the time variation of the local composition $x(r)$ to the flux $\partial x(r)/\partial t=-divJ(r)$. In this way, one obtains the standard diffusion equation for finding the concentration profile $x(r)$ which can be associated with a probability to find a diffusing particle at the point r. For the ordinary diffusion, the mean squared displacement obeys the standard Einstein relation $\langle r^2\rangle \propto Dt$. Quite often, the experimental data exhibit the power-law-dependence

$$Z(i\omega) \propto (i\omega)^{-\nu/2} \tag{45}$$

with the exponent deviating from 1/2. This process is associated [42] with the so-called anomalous diffusion for which $\langle r^2\rangle$ exhibits a power-law-dependence

$$\langle r^2 \rangle \propto \overline{D}t^{\nu} \tag{46}$$

In order to recover this result, either the conservation law or the constitutive relation must be modified to involve fractional derivatives or the composition in a given power. Such equations naturally arise for the diffusion with power-law memory kernels typical for systems involving structural complexity (e.g., amorphous materials or fractals). On the other hand, recall that the Fickian relation, implying that the composition gradient is the driving force, is valid only for low or near the saturation compositions. In general, the chemical potential should be considered as the driving force (see Eq. 6). Then, as we have seen above, apart from the purely kinetic part, the problem involves the thermodynamic part ($\partial\mu/\partial x$). Therefore, a non-standard impedance can result from a complex kinetics or from a non-standard (non-Gibbsian) thermostatistics. Indeed, it has been shown [49] that the Levi-like distribution, related to anomalous diffusion, can be

recovered as a result of slow temperature fluctuations in the system environment (reservoir). This suggests that the intercalation systems, apart from their technological importance, could also serve as promising examples for exploring new effects related to the non-standard thermostatistics.

The thermodynamics of intercalation into disordered matrices is analyzed in terms of the maximum entropy principle combined with the distortive lattice gas model. This approach allows us to account for the matrix volume expansion and the fluctuating internal distortions, seen in the recent experiments [53, 54]. Therefore, the crossover behavior from thin to thick films can be understood as a cooperative result of a threshold-like host volume variation with the guest concentration, x, and the internal distortions, optimizing the host–guest coupling. Our analysis points to the occurrence of the film support effect on the characteristic concentration x_0, corresponding to the volume dilatation onset. Decreasing thickness entails increasing x_0 values. A work on interpreting this tendency in terms of some physical film property is in progress. For instance, in the light of the present study, differences in the distorted amorphous structure (free volume) might be behind this effect. In order to verify this conjecture, a systematic experimental study of the concentration-dependent host morphology is desirable. This issue is left for a future study.

References

1. McKinnon WR, Haering RR (1983) In: White RE, Bockris JO'M (eds) Modern aspects of electrochemistry, vol 15. Plenum Publishing, New York, p 235
2. Schlapbach L, Zuttel A (2001) Nature (London) 414:353
3. Slusky JS et al (2001) Nature (London) 410:343
4. Berlinsky AJ, Unruh WG, McKinnon WR, Haering RR (1979) Solid State Comm 31:135
5. Coleman ST, McKinnon WR, Dahn JR (1984) Phys Rev B 29:4147
6. Strømme Mattsson M (1998) Phys Rev B 58:11015
7. Thompson AH (1978) Phys Rev Lett 40:1511
8. Hsu JP, Liu BT (1997) J Phys Chem B 101:7928
9. Vorotyntsev MA, Badiali JP (1994) Electrochim Acta 39:289
10. Laberge CA, Fratzl P, Lebowitz JL (1995) Phys Rev Lett 75:4448
11. Spencer BJ, Voorhees PW, Tersoff J (2000) Phys Rev Lett 84:2449
12. De Ninno A, Violante V, La Barbera A (1997) Phys Rev B 56:2417
13. Baranowski B (1989) J Less-Common Metals 154:329
14. Zoltowski P (1999) Electrochim Acta 44:4415
15. Zhang WS, Zhang XW, Zhang ZL (2000) Phys Rev B 62:8884
16. Zhong Q, Dahn JR, Colbow K (1992) Phys Rev B 46:2554
17. Gao Y, Reimers JN, Dahn JR (1996) Phys Rev B 54:3878
18. Zheng T, Dahn JR (1997) Phys Rev B 56:3800
19. Safran SA (1980) Phys Rev Lett 44:937
20. Bak P, Forgacs G (1985) Phys Rev B 32:7535
21. Dahn JR, Dahn DC, Haering RR (1982) Solid State Comm 42:179
22. Thorpe MF, Jin W, Mahanti SD (1989) Phys Rev B 40:10294
23. Fischer JE, Kim HJ (1987) Phys Rev B 35:3295
24. Whittingham MS (1976) J Electrochem Soc 123:315
25. Kaluarachchi D, Frindt RF (1985) Phys Rev 31:3648
26. Clerc DG, Poshusta RD, Hess AC (1997) J Phys Chem A 101:8926
27. McKinnon WR, Haering RR (1980) Solid State Ion 1:111
28. Larche FC, Cahn JW (1985) Acta Metall 33:331
29. Nauman EB, He DQ (2001) Chem Engineering Sci 56:1999
30. Vakarin EV, Badiali JP (1999) Phys Rev B 60:2064
31. Vakarin EV, Filippov AE, Badiali JP (1998) Phys Rev Lett 81:3904
32. Vakarin EV, Filippov AE, Badiali JP (1999) Surf Sci 422:L200
33. Vakarin EV, Badiali JP, Levi MD, Aurbach D (2001) Phys Rev B 63:014304
34. Vakarin EV, Badiali JP (2001) Electrochim Acta 46:4151
35. Vakarin EV, Badiali JP (2002) J Phys Chem B 106:7721
36. Vakarin EV, Badiali JP (2004) Solid State Ion 171:261
37. Kalikmanov VI, de Leeuw SW (2002) J Chem Phys 116:3083
38. Lee S, Miyazaki H, Mahanti SD, Solin SA (1989) Phys Rev Lett 62:3066
39. Molenda J, Kubik A (1999) Solid State Ion 117:57
40. Strømme Mattsson M (2000) Solid State Ion 131:261
41. Levi MD, Aurbach D (1997) J Phys Chem B 101:4641
42. Bisquert J, Compte A (2001) J Electroanal Chem 499:112
43. Sasaki S, Maeda H (1996) Phys Rev E 54:2761
44. Matsuda R et al (2005) Nature (London) 436:238
45. Julien CM (2003) Mater Sci and Engineering R 40:47
46. Gelb LD, Gubbins KE, Radhakrishnan R, Sliwinska-Bartowiak M (1999) Rep Prog Phys 62:1673
47. Kudo T, Hibino M (1996) Solid State Ion 84:65
48. Detcheverry F, Kierlik E, Rosinberg ML, Tarjus G (2005) Phys Rev E 72:051506
49. Vakarin EV, Badiali JP (2006) Phys Rev E 74:036120
50. Escobedo FA, de Pablo JJ (1997) J Chem Phys 106:793
51. Odriozola G, Aguilar JF (2005) J Chem Phys 123:174708
52. Thibault P, Prejean JJ, Puech L (2005) Phys Rev B 52:17491
53. Garcia-Belmonte G, Garcia-Canadas J, Bisquert J (2006) J Phys Chem B 110:4514
54. Garcia-Belmonte G, Vikhrenko VS, Garcia-Canadas J, Bisquert J (2004) 170:123
55. Vakarin EV, Duda Y, Badiali JP (2006) J Chem Phys 124:144515
56. Vakarin EV, Duda Y, Badiali JP (2007) J Phys Chem B 111:2540
57. Vakarin EV, Badiali JP (2005) Electrochim Acta 50:1719
58. Jaynes ET (1957) Phys Rev 106:620
59. Vakarin EV, Badiali JP (2004) Surf Sci 565:279
60. Vakarin EV, Badiali JP (2002) Surf Sci 513:431